Published in final edited form as:
Sci Transl Med. 2010 March 17; 2(23): 23ra19. doi:10.1126/scitranslmed.3000678.

Targeting Robo4-Dependent Slit Signaling to Survive the Cytokine Storm in Sepsis and Influenza

Nyall R. London[1,2,3,*], **Weiquan Zhu**[1,2,3,*], **Fernando A. Bozza**[4], **Matthew C. P. Smith**[1,2,3], **Daniel M. Greif**[5,6], **Lise K. Sorensen**[1,2,3], **Luming Chen**[1,2,3], **Yuuki Kaminoh**[1,2,3], **Aubrey C. Chan**[1,2,3], **Samuel F. Passi**[1,2,3], **Craig W. Day**[7], **Dale L. Barnard**[7], **Guy A. Zimmerman**[2], **Mark A. Krasnow**[5], and **Dean Y. Li**[1,2,3,†]

[1]Department of Oncological Sciences, University of Utah, Salt Lake City, UT 84112, USA.

[2]Department of Medicine, University of Utah, Salt Lake City, UT 84112, USA.

[3]Program in Molecular Medicine, University of Utah, Salt Lake City, UT 84112, USA.

[4]Intensive Care Unit, Instituto de Pesquisa Clínica Evandro Chagas, and Laboratório de Imunofarmacologia, Fundação Oswaldo Cruz, Rio de Janeiro 21045-900, Brazil.

[5]Department of Biochemistry and Howard Hughes Medical Institute, Stanford University School of Medicine, Stanford, CA 94305, USA.

[6]Department of Medicine, Division of Cardiovascular Medicine, Stanford University School of Medicine, Stanford, CA 94305, USA.

[7]Institute for Antiviral Research, Utah State University, Logan, UT 84322, USA.

Abstract

The innate immune system provides a first line of defense against invading pathogens by releasing multiple inflammatory cytokines, such as interleukin-1β and tumor necrosis factor–α, which directly combat the infectious agent and recruit additional immune responses. This exuberant cytokine release paradoxically injures the host by triggering leakage from capillaries, tissue edema, organ failure, and shock. Current medical therapies target individual pathogens with antimicrobial agents or directly either blunt or boost the host's immune system. We explored a third approach: activating with the soluble ligand Slit an endothelium-specific, Robo4-dependent signaling pathway that strengthens the vascular barrier, diminishing deleterious aspects of the host's response to the pathogen-induced cytokine storm. This approach reduced vascular permeability in the lung and other organs and increased survival in animal models of bacterial endotoxin exposure, polymicrobial sepsis, and H5N1

†To whom correspondence should be addressed. dean.li@u2m2.utah.edu.
*These authors contributed equally to this work.

Author contributions: N.R.L., W.Z., and D.Y.L. were responsible for project conceptualization, experimental design, and data analysis. N.R.L., G.A.Z., and D.Y.L. were responsible for manuscript preparation. N.R.L., W.Z., and F.A.B. were responsible for performing all experiments or coordinating experimental design and work of others. M.C.P.S., D.M.G., L.K.S., L.C., Y.K., A.C.C., and S.F.P. performed necessary experiments for the manuscript or in response to reviewers. C.W.D., D.L.B., G.A.Z, and M.A.K. provided important expertise, reagents, technical personnel and advice.

Competing interests: N.R.L., W.Z., M.C.P.S., L.K.S., L.C., Y.K., S.F.P., G.A.Z., and D.Y.L. are or were previously employed by the University of Utah, which has filed intellectual property surrounding the therapeutic uses of targeting Robo4 and with the intent to license this body of intellectual property for commercialization. The University of Utah has licensed Robo4 technology to Navigen, a biotechnology company owned in part by the University of Utah Research Foundation. N.R.L. and W.Z. are paid consultants for Navigen, and D.Y.L. is a founder of and is on the Board of Directors of Navigen.

influenza. Thus, enhancing the resilience of the host vascular system to the host's innate immune response may provide a therapeutic strategy for treating multiple infectious agents.

INTRODUCTION

The devastating consequences of influenza epidemics, the poor medical outcome after sepsis, and the emergence of new infectious pandemic and biowarfare threats have kindled interest in the development of broad-spectrum strategies that can be rapidly implemented by public health and military defense agencies (1,2). There are now two main ways to address these infectious threats. The first is to target specific pathogens with antimicrobials. With this approach, time is required to identify the specific pathogen once a pandemic has emerged. In addition, pathogens often mutate, developing resistance to antibiotics and antiviral agents (3,4). The recent emergence of a pandemic influenza strain highlights these limitations (5).

A second approach is to modulate the host's innate immune system (6). Innate immunity provides the host with immediate protection against a broad and unforeseen spectrum of pathogens. When activated by endotoxin [lipopolysaccharide (LPS)] or other microbial components, this system, which is composed of neutrophils, monocytes, macrophages, Langerhans cells, dendritic cells, and natural killer cells, releases multiple cytokines with broad antibacterial and antiviral properties as well as regulatory effects on subsequent adaptive immune responses. The marked and abrupt release of multiple cytokines by the immune system, often referred to as hypercytokinemia or cytokine storm, itself has disruptive effects on the host's physiology. In many infections, components of the resulting cytokine-induced secondary inflammatory injury can be more toxic than the invading microbes themselves (7). Inflammatory cytokines, such as tumor necrosis factor (TNF) and interleukin-1β (IL-1β), destabilize endothelial cell-cell interactions and cripple vascular barrier function, resulting in capillary leakage, tissue edema, organ failure, and death (5,8,9). These phenomena occur in septic shock, acute lung injury, and acute respiratory distress syndrome—all common endpoints in patients exposed to serious infections (for example, the 1918 influenza pandemic). The prominent role of cytokines in these pathologies has led to the testing of agents that reduce cytokine signaling as possible therapeutics (10). This clinical strategy has, however, been disappointing, often resulting in increased mortality (11–13). The converse strategy of boosting the immune system with infusion of inflammatory cytokines has also been advocated, but its clinical use has been limited because of undesirable outcomes (6). For example, delivery of ILs to treat melanoma precipitates aseptic vasogenic shock in patients (14). Thus, for survival of the infected patient or animal, a balance must be struck between a protective innate immune response that eliminates the pathogen and an excessive immune response that injures the host.

Here, we have explored a third approach: maximizing the host's endogenous ability to overcome infectious challenge by limiting the disruptive effects of proinflammatory mediators on the vasculature. By augmenting the resilience of the host's vascular system to cytokines, we sought to enable the body to endure an excessive innate immune response. We identified the Slit-induced signaling pathway as a modulator of vascular stability that can strengthen endothelial cell-cell interactions. Activation of this pathway is effective in reducing capillary leak, multiorgan edema, and death in multiple animal models of infections, including H5N1 influenza.

RESULTS

Slit regulates vascular endothelial cadherin localization

Because the vascular system is exposed to ischemic, infectious, and inflammatory stresses, the endothelium is continuously challenged by angiogenic factors, inflammatory mediators, and

permeability agents. All of these molecules disrupt the endothelial barrier of the mature vascular system and contribute to the classic findings of calor (heat), dolor (pain), rubor (redness), and tumor (swelling) on inflammation. Members of the Slit family of neurovascular guidance cues inhibit vascular endothelial growth factor (VEGF)–induced vascular hyperpermeability in a process dependent on the endothelial-specific receptor Robo4 (15). This inhibition of VEGF signaling by Slit protein is mediated through the small intracellular guanosine triphosphatase, Arf6 (16). Because Robo4 messenger RNA concentrations increase in response to a diverse repertoire of angiogenic (15,17,18) and inflammatory exposures, we hypothesized that Robo4 may be part of a vascular stability signaling program. We tested this hypothesis by examining whether Robo4-dependent Slit signaling reduces the endothelial hyperpermeability induced by endotoxin (LPS), TNF-α, and IL-1β, all important mediators of inflammation (19). To study barrier function in vitro, we assessed the ability of a human endothelial cell monolayer to act as a barrier to diffusion of a horseradish peroxidase reporter. We used the N-terminal fragment (Slit2N), which is the active fragment of Slit that is released by proteolytic cleavage (20). Slit2N at 10 nM substantially reduced LPS-induced, TNF-α–induced, and IL-1β–induced permeability (Fig. 1A) but did not significantly affect basal permeability (fig. S1A). Furthermore, the inhibitory effect of Slit2N was lost in cells exposed to small interfering RNA (siRNA) directed against Robo4 but not in those exposed to control scrambled siRNA (Fig. 1B and fig. S1B).

Because Robo4-dependent Slit2N signaling tempers the effects of such a range of angiogenic and inflammatory cytokines (Fig. 1A), we tested whether this pathway promotes vascular stability by directly enhancing the molecular machinery responsible for cell-cell interactions. In the endothelium, critical intercellular interactions are mediated by the adherens junction protein vascular endothelial cadherin (VE-cadherin) (21,22). When we treated human microvascular lung endothelial (HMVEC-lung) cells with Slit2N, VE-cadherin abundance was significantly increased at the cell surface junctions (Fig. 1, C and F, and fig. S1C). VE-cadherin presence on the cell surface is regulated by the association of p120-catenin with VE-cadherin, an association that inhibits VE-cadherin internalization from the cell surface and promotes vascular stability (23,24). Slit2N also increased the cell surface abundance of p120-catenin (Fig. 1D) but had no effect on β-catenin (Fig. 1E).

Next, we determined whether Slit2N affected VE-cadherin at the cell surface after exposure to IL-1β. IL-1β reduced VE-cadherin at the cell surface, and Slit2N negated this effect (Fig. 2A). IL-1β stimulation decreased p120-catenin at the cell surface, and Slit2N reversed this effect (Fig. 2A). IL-1β induced dissociation of VE-cadherin from p120-catenin and internalization of VE-cadherin (Fig. 2, B and C). Slit2N restored the association of VE-cadherin and p120-catenin and blocked internalization of VE-cadherin (Fig. 2, B and C). VE-cadherin internalization experiments were performed in the presence of primaquine to prevent endocytic recycling (25). In the absence of primaquine, we were unable to detect IL-1β–induced VE-cadherin internalization (fig. S1D). It has been proposed that phosphorylation of VE-cadherin at Tyr^{658} disrupts its binding to p120-catenin and results in the endocytosis of VE-cadherin (23). Our experiments indicate that Slit2N stabilized the interaction between VE-cadherin and p120-catenin by inhibiting IL-1β–induced phosphorylation of VE-cadherin at Tyr^{658} (fig. S1E).

Next, we investigated whether the effect of Slit2N on VE-cadherin localization is necessary for its ability to enhance vascular stability. Because VE-cadherin siRNA had a potent disruptive effect on the endothelial monolayer at baseline (fig. S1, F and G), we used an antibody to VE-cadherin to block the effect of Slit2N on permeability in vitro. Slit2N inhibited IL-1β–induced permeability in vitro in the presence of a nonspecific immunoglobulin G (IgG); however, the effect of Slit2N was lost in the presence of an antibody to VE-cadherin (Fig. 2D). Together, these data suggest that Slit2N preserves the association of p120-catenin with VE-cadherin in

the face of IL-1β stimulation and thereby promotes vascular integrity by reducing cytokine-induced VE-cadherin endocytosis.

Slit enhances vascular stability in vivo

To examine whether Slit reduces permeability under conditions of cytokine storm in vivo, we used a bacterial endotoxin model of pulmonary inflammation. In this model, LPS is administered to the lungs of mice through intratracheal instillation, simulating a Gram-negative infection (26). LPS administration triggers a massive inflammatory reaction and release of cytokines, resulting in a large increase in alveolar capillary permeability. Using Evans blue albumin (EBA) as a tracer, we found that Slit2N significantly reduced vascular leak in the lungs of LPS-treated *Robo4*$^{+/+}$ mice (Fig. 3A). The effect of Slit2N was lost in *Robo4*-null (*Robo4*$^{AP/AP}$) mice, showing that Robo4 is necessary for the effect of Slit2N in vivo (Fig. 3A). This result also indicates that this activity is endothelial-specific, as Robo4 is only detected in the endothelium (17,18). LPS instillation in the lung also induces accumulation of protein exudates and leukocytes in the alveolar space, inflammatory responses that can be quantified in bronchoalveolar lavage fluid (BALF) (26). Slit2N reduced protein exudate, a key marker of acute lung injury and indicator of vascular barrier disruption (10), and inflammatory cell accumulation in the BALF of *Robo4*$^{+/+}$ mice in a dose-dependent manner (Fig. 3, B to D, and fig. S2, A and B). The Slit2N-induced inhibition of protein and leukocyte accumulation in BALF was lost in *Robo4*$^{AP/AP}$ mice, indicating again that Slit2N acts directly on the vasculature to decrease protein exudates and inflammatory cell accumulation in the alveoli (Fig. 3, B to D). Finally, histological examination of the lung confirmed that Slit2N acts in a Robo4-dependent manner by reducing LPS-induced lung inflammation in *Robo4*$^{+/+}$ but not *Robo4*$^{AP/AP}$ mice (Fig. 3E and fig. S2C). Because neutrophils are a predominant cell type in bacterial pneumonia and LPS challenge models (26), we tested whether Slit2N had a direct effect on neutrophil migration. Primary human polymorphonuclear leukocytes (hPMNs) did not respond to Slit2N, consistent with the fact that they do not express Robo receptors (fig. S3, A and B).

One might anticipate that the loss of Robo4 would make mice more sensitive to LPS exposure, but in initial studies, we did not detect enhanced sensitivity in the lungs of *Robo4*$^{AP/AP}$ mice relative to *Robo4*$^{+/+}$ mice (Fig. 3, B to D). We reasoned that if the amount of LPS administered was too large, it could cause such severe damage that any difference between the two genotypes would be masked. Thus, we lowered the dose of LPS used to challenge the mice and, under these conditions, found that *Robo4*$^{AP/AP}$ mice exhibited significantly higher protein concentrations in BALF than did littermate *Robo4*$^{+/+}$ mice (Fig. 3F). This increased sensitivity of *Robo4*$^{AP/AP}$ mice to LPS suggests that endogenous Robo4-dependent Slit signaling normally dampens the effects of cytokines on the vasculature. Consistent with this suggestion, Slit2 protein is expressed throughout the lung and in close proximity to the endothelium (fig. S4).

To determine whether Slit acts via a VE-cadherin–dependent mechanism in vivo, we blocked VE-cadherin with a specific antibody that prevents homophilic interactions between VE-cadherin expressed on adjacent endothelial cells (27). Slit2N reduced protein exudates and inflammatory cell infiltration in the presence of a control IgG antibody but not in the presence of a VE-cadherin–blocking antibody (Fig. 3, G to I). Thus, as in our cell culture experiments, our in vivo experimental results support the idea that Slit2N promotes VE-cadherin expression at the cell surface, which blunts cytokine-mediated endothelial hyperpermeability.

Enhancing vascular stability during polymicrobial sepsis

To evaluate whether Slit2N can reduce mortality in the setting of systemic vascular instability, and whether the effect of Slit2N is limited to the lung, we used a model of polymicrobial sepsis

known as cecal ligation and puncture (CLP) (28). Slit2N significantly reduced vascular permeability in the kidney and spleen (Fig. 4, A and B) and improved the survival of mice exposed to CLP-induced sepsis from 33 to ~80% (Fig. 4C). Under the conditions of these experiments, CLP did not cause significant damage to the lung (fig. S5, A to C). Because a hyper-inflammatory response contributes to the pathogenesis of sepsis, we also tested whether Slit2N could affect cytokine and chemokine concentrations in the plasma of septic mice (19). Slit2N did not alter plasma concentrations of a panel of cytokines and chemokines, demonstrating that the therapeutic effect of Slit2N is not secondary to a reduction in inflammatory cytokine and chemokines (Fig. 4, D and E). The effect of Slit2N on mortality after CLP treatment was lost in *Robo4*$^{AP/AP}$ mice (Fig. 4F), hence Robo4 is necessary for this activity of Slit2N. Additionally, the loss of Robo4 did not alter cytokine receptor levels, nor does Slit2N inhibit cytokine receptor activation or induce Robo4 expression in endothelial cells (fig. S6, A and B). Together, these data demonstrate that Slit can enhance survival by specifically enhancing vascular stability during the systemic inflammatory response triggered by sepsis.

Stabilizing the vasculature reduces mortality after H5N1 infection

LPS instillation and CLP mimic the vascular instability and dysregulated inflammation induced by bacterial pathogens. To determine whether a therapeutic strategy of vascular stabilization can be productively applied to viral infections, we examined the effects of Robo4-dependent Slit2N treatment in a model of H5N1 influenza. Pandemic influenzas such as avian flu (H5N1) provide extreme examples of infection-induced lung injury characterized by large increases in cytokine concentrations and excessive inflammation (29–31). Slit2N significantly inhibited endothelial hyperpermeability in the lung 3 days after H5N1 infection of mice (Fig. 5A) and also reduced mortality (Fig. 5B). The lung pathology in Slit2N-treated mice was less severe than it was in mock-treated mice (Fig. 5C). To exclude the possibility that Slit2N has direct antiviral activity, we measured lung viral titers and found that Slit2N did not alter viral load (Fig. 5D); further, Slit2N did not significantly reduce the amount of inflammatory cytokine released in the lung after H5N1 infection (Fig. 5, E and F). These results are consistent with our LPS and CLP studies and indicate that limiting the vascular response to hypercytokinemia is sufficient to reduce mortality and morbidity in animal models of serious infection.

DISCUSSION

Pandemic influenza and bacterial sepsis are infections that have sizable mortality rates and substantially affect public health (32). New ways to address these constantly evolving biological threats are needed (33). Here, using rodent models of infection, we have demonstrated that cytokine storm and capillary leakage contribute to the poor outcome of endotoxin-induced acute lung injury, polymicrobial sepsis, and pandemic influenza. We further show that administration of the exogenous ligand Slit2N strengthens the endothelial barrier and blunts vascular leak in response to cytokine storm (Fig. 6). Exogenously applied Slit2N stabilizes cell surface VE-cadherin, a primary molecular determinant of intact barrier function in the endothelium, and this strengthened barrier can protect mice from the lethal effects of sepsis or influenza infection. Furthermore, in genetically modified mice lacking Robo4, Slit2N cannot prevent vascular leakage in infection or sepsis, indicating that Robo4 is a critical mediator of Slit-promoted vascular stability.

We and others have long assumed that Robo4 played an essential role in development based on a number of observations, including the role of Slit-Robo signaling in neuronal guidance (34) and the lethality of mutations in genes of this signaling pathway (35–37). Yet, unexpectedly, mice homozygous for null mutations of *Robo4* are viable (15). Similarly, in a

detailed characterization of lung development, we could find no structural differences between *Robo4*$^{AP/AP}$ (null) mice and their wild-type sibling controls (fig. S7 and fig. S8).

Our results suggest an alternative function for Robo4: This receptor may be important for modulating the vascular response to inflammatory cytokines but not for development. As with other pathways that maintain adult homeostasis, including many involved in the immune response, one cannot a priori expect that these pathways are also essential for development. Genetic alterations in these pathways might only manifest after exposure to physiologic or environmental stress (38).

In our experiments, we tested one way that signaling via Robo4 could modulate critical host inflammatory responses. Because Slit2 affects migration of dimethyl sulfoxide (DMSO)–treated HL-60 cells, a promyelocytic leukemia cell line often used as a surrogate for primary neutrophils (39), we asked whether Slit2 inhibits migration of neutrophils, which could account for the reduced numbers of inflammatory cells in the lungs of LPS-treated mice (40). Although in our hands Slit2 also inhibited migration of DMSO-treated HL-60 cells, we found no evidence that primary hPMNs respond to Slit2N, nor do they express Robo receptors (fig. S3, A and B).

Rather, our data demonstrate that Robo4 is required for the effect of Slit2N on VE-cadherin–mediated vascular barrier function. Similarly, expression of either Robo4 or Robo1 is necessary and sufficient to make cells sensitive to Slit (15,16,18,39,41). The simplest interpretation of these data would be that Slit2 acts as a direct ligand for Robo4. This may not be the case, however. Others have postulated that co-receptors such as syndecans are required for the function of Robo receptors in neural guidance (42–45). Western blot and immunoprecipitation studies in the presence of non-denaturing detergents (0.5% NP-40) reveal specific binding of Slit2 to Robo4 (18), but the use of harsher conditions using ionic denaturing detergents (1% Triton X-100–0.5% deoxy-cholate) fails to preserve this interaction (46). To reconcile this variable and detergent-dependent binding between Slit2 and cell surface Robo4, the absence of strong interaction between Slit and Robo4 in an in vitro Biacore assay (46), and the strong signaling and functional response of Robo4 to Slit, Sheldon *et al*. (42) and Suchting *et al*. (46) propose that Robo4 and Robo1 receptors form a heterodimeric complex in human vein endothelial cells and show that the Robo1 and Robo4 receptors bind to one another. Consistent with their model, we find that knockdown of either Robo4 or Robo1 abrogates the ability of Slit to inhibit migration of human vein endothelial cells (fig. S9). Further investigation of the roles of Robo1 and syndecans as co-receptors for Robo4 is needed.

The endothelial cell monolayer provides a critical semipermeable barrier between the blood and tissue that regulates the passage of nutrients, fluid, and leukocytes into the interstitial space (47). The integrity of this barrier is determined by homophilic interactions between the cell surface adherens junction protein VE-cadherin on adjacent endothelial cells (48). In states of active angiogenesis or acute inflammation, cytokines induce rapid endocytosis of VE-cadherin, disrupting the transcellular homophilic binding of VE-cadherins, deconstructing paracellular adherens junctions, and resulting in hyperpermeability (21,49–51). Our study suggests that the destabilizing effects of angiogenic and inflammatory cytokines are opposed by extracellular cues that promote vascular stability. Although two stabilizing regulators of the vascular barrier, Tie2-dependent angiopoietin signaling and Robo4-dependent Slit signaling, use different immediate downstream signaling cascades, both ultimately blunt cytokine-mediated endocytosis of cell surface VE-cadherin (15,16,52). Thus, the strength of the endothelial barrier may be a product of a constant tug-of-war between opposing stabilizing and destabilizing signals that control VE-cadherin trafficking, allowing the vascular system the necessary plasticity to respond to changing physiologic needs.

The innate immune system provides the first line of defense of the body against pathogens and must be rapid, broad-spectrum, and toxic to the offending pathogen. There is a fine line between overwhelming the invaders and inflicting severe collateral damage to the host. Boosting the innate immune system with cytokines increases the risk of vasogenic shock, yet efforts to reduce secondary damage by suppressing the innate immune response with glucocorticoids can worsen the outcomes from severe infection. Thus, pharmacologic modulation of the innate immune response has a narrow therapeutic window.

The specific cytokines elaborated and their temporal secretion profile may differ for each pathogen. Nevertheless, the cumulative effects of hypercytokinemia on vascular leakage and noncardiogenic shock are common among severe infections characterized by septic shock (29,30,53). Our data suggest that an alternative approach to combating these infections is to strengthen the vascular barrier. The pharmacologic promotion of vascular stability was sufficient to mute the vascular hyperpermeability induced by multiple different cytokines and the subsequent mortality in rodent models of severe bacterial and viral infections. Enhancing stability offers practical advantages over a more complicated approach aimed at blocking each individual cytokine contributing to cytokine storm. The practical success of targeting the vascular response to cytokines may require a careful characterization of the temporal sequence involving infection, hypercytokinemia, vascular leakage, organ failure, and eventual death (9,29,30,54). A likely limitation is that this therapeutic approach may need to be used before the vascular damage is too grave to repair. Even so, targeting the host and not the pathogen offers a stratagem that could offer sufficient flexibility to successfully combat ever-changing biologic threats from drug-resistant, mutating, and emerging infectious agents (55).

MATERIALS AND METHODS

Preparation of recombinant Slit2N

293T cells plated onto poly-L-lysine (Sigma)–coated dishes were transiently transfected with empty vector pSecTagB or pSecTagB::hSlit2N. For each 15-cm dish of cells, 60 μg of DNA and 100 μl of Lipofectamine (Invitrogen) in serum-free Opti-MEM were used. Slit2N protein was salt-extracted as described (15). Using this protocol, we obtained Slit2N concentrations of 0.5 to 1.5 mg/ml. We performed the same salt extraction procedure on cells transfected with empty vector pSecTagB. This preparation is referred to as Mock and was used as a control for Slit2N in all experiments. In vitro studies were conducted with 10 nM Slit2N.

In vitro permeability assay

In vitro permeability testing was performed as described (15) with LPS (100 ng/ml; serotype 0111:B4; Sigma) for 3 hours, TNF-α (10 ng/ml; R&D Systems) for 6 hours, or IL-1β (10 ng/ml; R&D Systems) for 2 hours. As indicated, this was repeated in the presence of control rabbit IgG (25 μg/ml; Jackson ImmunoResearch) or antibody to human VE-cadherin (25 μg/ml; RDI Fitzgerald). Basal permeability for unstimulated monolayers was set at 100%. Data are presented as mean ± SEM of at least three independent experiments performed in triplicate.

Robo4 siRNA knockdown

huRobo4 siRNA duplex (Hs_Robo4_1_HP; Qiagen) or equimolar All-Stars Negative Control siRNA (Qiagen) transfection complexes were formed according to standard protocol and added to the upper chamber of Transwell filters. Twenty-four hours later, cells were transfected a second time with huRobo4 or control siRNA. After an additional 24 hours, in vitro permeability was assessed as described. Data are presented as mean ± SEM of at least three independent experiments performed in triplicate. Successful knockdown of Robo4 protein expression was confirmed by Western blot with antibodies against Robo4 (N-17) or β-tubulin (Santa Cruz Biotechnology).

Subcellular fractionation

HMVEC-lung cells were treated with Slit2N or Mock in 0.1% fetal bovine serum (FBS) EBM-2 for 1.5 hours. Cells were then washed twice with ice-cold phosphate-buffered saline (PBS) containing Ca^{2+}-Mg^{2+} and once with HLB buffer [10 mM tris-HCl (pH 7.4), 5 mM KCl, and 1 mM $MgCl_2$] and collected in HLB buffer supplemented with protease inhibitors (Roche), phosphatase inhibitors (Sigma), and 1 mM dithiothreitol (DTT). Cells were then homogenized in a Dounce homogenizer (20 strokes). The homogenate was centrifuged at 400*g* for 10 min at 4°C to pellet cell debris. The resulting supernatant was centrifuged again at 16,000*g* for 30 min at 4°C. The pellet was washed once with HLB and resuspended in radioimmunoprecipitation assay (RIPA) buffer for 30 min at 4°C. The resuspended pellet was centrifuged (16,000*g* for 15 min at 4°C), and the resulting supernatant was saved as a soluble membrane fraction. To obtain the total cell lysate, we saved an aliquot before Dounce homogenization. RIPA buffer was added to this aliquot and centrifuged at 13,000*g* for 10 min at 4°C. The supernatant was saved and used as total cell lysate. Antibodies to VE-cadherin were obtained from Cell Signaling, and p120-catenin and β-catenin were from BD Biosciences. Densitometry was performed on at least three independent experiments and data are presented as mean ± SEM.

Immunofluorescence

Immunofluorescence was performed as described (15). Cells were pretreated with Slit2N or Mock for 30 min followed by stimulation with IL-1β (10 ng/ml) for 3 hours. Primary antibodies to VE-cadherin (BD Biosciences) or p120-catenin (Santa Cruz Biotechnology) were applied at 4°C overnight. Images are representative of three independent experiments.

Immunoprecipitation

HMVEC-lung cells (Lonza) were treated with Slit2N or Mock in 0.1% FBS EBM-2 for 30 min. Cells were then stimulated with IL-1β (10 ng/ml) for 10 min. HMVEC-lung cells were then washed with ice-cold PBS and lysed with ice-cold lysis buffer [10 mM tris-HCl (pH 7.4), 50 mM NaCl, 1% NP-40, and 10% glycerol] supplemented with protease inhibitors, phosphatase inhibitors, and 1 mM DTT. Cell lysates were incubated on ice for 30 min and centrifuged at 13,000*g* for 15 min to pellet cell debris. Protein concentrations were determined by BCA assay (Pierce), and 0.5 mg of lysate was incubated with 8 μg of VE-cadherin antibody (Cell Signaling) and protein A/G–Sepharose (Santa Cruz Biotechnology) for 1 hour at 4°C. Complexes were washed three times with lysis buffer. The immunoprecipitates were subjected to Western blot analysis using a 95% fraction of the immunoprecipitate for the p120-catenin blots and the remaining 5% fraction for the VE-cadherin blots (Fig. 2B). Densitometry was performed on three independent experiments, and data as a ratio of immunoprecipitated p120-catenin to loaded VE-cadherin are presented as mean ± SEM.

Internalization assay

VE-cadherin internalization was performed as described (24). In brief, HMVEC-lung cells were seeded onto chamber slides and cultured for 72 hours. The media were then removed, and the cells were labeled for 30 min at 4°C with an antibody to VE-cadherin (clone BV6; RDI Fitzgerald). Cells were then pretreated with Slit2N or Mock for 30 min. Excess antibody was removed by washing twice on ice with ice-cold media. Chamber slides were moved to 37°C and incubated for 1 hour with IL-1β (10 ng/ml) and 0.6 mM primaquine in the presence of 10 nM Slit2N or Mock. Cells were acid-washed to strip the surface-bound VE-cadherin. Monolayers were washed, fixed, and permeabilized. Internalized VE-cadherin antibody was detected with Alexa 488–conjugated donkey antibody to mouse IgG (Molecular Probes). Images are representative of four independent experiments.

Animals

The Institutional Animal Care and Use Committee at the University of Utah or at Utah State University approved the following animal protocols. *Robo4*$^{AP/AP}$ mice have been described (15).

LPS-induced acute lung injury

Eight- to 12-week-old C57BL/6 mice were injected intravenously with saline alone or 3.5 μg of Slit2N or Mock in saline. Alternatively, the intravenous injection also contained 20 μg of control IgG or 20 μg of VE-cadherin–blocking antibody (clone BV13; eBiosciences). Animals were anesthetized with Avertin before surgical exposure of the trachea. LPS (10 μg; serotype 0111:B4) in 100 μl of saline or saline alone was administered intratracheally. Twenty-four hours later, the trachea was reexposed and catheterized. BALF was obtained by injection of saline (1 ml) followed by aspiration repeated three times. BALF was centrifuged at 300*g* for 5 min to recover inflammatory cells. The pellet was treated with ACK buffer for 3 min to remove red blood cells. Cells were centrifuged at 300*g* for 5 min and resuspended in 1 ml of PBS containing 1% FBS. Cell counts were then determined by hemocytometer. Neutrophil counts were determined by cell differential counts. A white blood cell differential was achieved by staining an aliquot of cells followed by microscopic examination to determine the percentage of the cell population that were neutrophils. BALF protein was assessed by protein assay (Bio-Rad). Data are presented as SEM of at least five mice per condition.

CLP sepsis model

Seven- to 11-week-old male C57BL/6 mice were given an intraperitoneal injection of 5 μg of Slit2N or Mock. One hour later, mice were anesthetized with isoflurane, and CLP was performed as described (56). Mice continued to receive an intraperitoneal injection of 5 μg of Slit2N or Mock once a day. Mice in the sham operation group were subjected to identical procedures, except that ligation and puncture of the cecum were omitted. Survival rate of mice subjected to CLP was determined for 6 days, with $n = 14$ for Slit2N treatment and $n = 15$ for Mock treatment for *Robo4*$^{+/+}$ mice. For *Robo4*$^{AP/AP}$ mice, $n = 13$ for Slit2N treatment and $n = 13$ for Mock treatment.

H5N1 infection

Female, 18 to 20 g, BALB/c mice (Charles River Laboratories) were anesthetized and infected with H5N1 virus (Influenza A, Duck/MN/1525/81) intranasally. Mice were given an intravenous injection of 1.56 μg of Slit2N or Mock daily for 5 days. Survival rate of mice subjected to H5N1 lung infection was determined for 21 days with 20 mice per condition.

Evans blue permeability

Vascular permeability in the lung was assessed with EBA as described (57). Five hours after intratracheal instillation of LPS, 4 hours after CLP, and 3 days after H5N1 infection, mice were given an intravenous injection of EBA (20 mg/kg). EBA was allowed to circulate for 1 hour, and mice were deeply anesthetized and perfused with saline plus 5 mM EDTA. Lungs were excised, weighed, and homogenized in 2 ml of PBS. Formamide (4 ml; Invitrogen) was added, and the samples were incubated overnight at 60°C to extract Evans blue dye. The samples were then centrifuged, and supernatants were analyzed by spectrophotometry at both 620 and 740 nm. CLP-treated mice were perfused, and their kidneys and spleen were removed, weighed, and placed in formamide for 48 hours at 60°C. The absorbances were normalized as described (57) and converted to microgram Evans blue dye per gram wet weight of lungs, kidneys, or spleen, respectively. Data are presented as SEM of at least four mice per condition.

Histology

Twenty-four hours after LPS exposure or CLP, mice were killed by CO_2 asphyxiation. Chest cavities were opened, and lungs were inflated with $ZnSO_4$-buffered 10% formalin. Formalin-fixed tissues were processed routinely, embedded in paraffin, sectioned at 6 μm, and stained with hematoxylin and eosin (H&E). Histologic quantification was modified from methods described (58). For H5N1 samples, 6 days after infection, the right lobes of the lungs from two animals were harvested and fixed in 10% neutral-buffered formalin. Formalin-fixed tissues were processed routinely, embedded in paraffin, sectioned at 5 μm, stained with H&E, and evaluated for microscopic lesions by a board-certified veterinary pathologist.

Lung immunofluorescence

Adult *Robo4*$^{+/AP}$ mice were killed by CO_2 asphyxiation. Chest cavities were opened, and lungs were inflated with optimum cutting temperature (OCT) embedding compound and frozen quickly in OCT on dry ice. Lung sections were stained for alkaline phosphatase activity, denoting areas of Robo4 expression as described (15). Sections were then stained with primary antibodies against Slit2 (E-20; Santa Cruz Biotechnology) or CD31 (BD Pharmingen) followed by fluorescent secondary antibody staining.

Cytokine or chemokine array

Six hours after CLP, mice were heavily anesthetized. Whole blood was drawn into acid-citrate-dextrose solution (ACD) (~1:9 volume) from the carotid artery. Plasma was isolated by centrifugation of blood at 4000*g* for 10 min. Plasma was analyzed by Quansys Biosciences to quantify cytokine and chemokine levels. Data are presented as mean ± SEM of six mice per condition. For H5N1 samples, 6 days after infection, clarified mouse lung homogenates were prepared and inflammatory cytokine and chemokine profiles were determined with mouse cytokine and chemokine arrays (Quansys Biosciences). Data are presented as mean ± SEM of three groups of pooled mice.

Lung virus titer determination

These assays were performed as described (59).

Lung development

Embryos were dissected, fixed, and rehydrated as described (60). Lungs were serially immunostained with primary antibody to platelet endothelial cell adhesion molecule (clone MEC 13.3; BD Pharmingen) and primary antibody to E-cadherin (clone ECCD-2; Zymed) with a variation of the described method (60).

Neutrophil migration

HL-60 cells were grown under standard conditions with RPMI 1640 supplemented with 10% FBS and 1% penicillin–streptomycin. Cells induced with 1.2% DMSO were obtained by seeding HL-60 cells at 3×10^6 per milliliter in growth media and culturing for 4 to 6 days (61). Human PMNs were isolated from healthy adult donor whole blood with ACD using techniques previously described (62). The leukocyte chemoattractant *N*-formyl-Met-Leu-Phe (*f*MLP) (10 μM), along with Slit2 or Mock, was placed in the lower wells of a 48-well chemotaxis chamber (Neuroprobe). A fibronectin-coated (overnight at 4°C) polycarbonate membrane (5 μm; Neuroprobe) was placed between the chemoattractant and the cells. HL-60 cells induced with DMSO or hPMNs (50 μl, 50,000 cells) were added to the upper wells. After incubating at 37°C for 2 hours, cells on the top surface of the filter were removed and cells that had migrated through the filter onto the undersurface were fixed and stained using Diff-Quik stain set (Dade Behring). Migrated cells in five high-power fields were counted and

migration was expressed as the percent of cells migrated relative to cells migrated toward *f*MLP in the absence of Slit2 or Mock. Data are presented as SEM of at least three independent experiments.

Quantitative polymerase chain reaction

For hPMN studies, RNA was isolated using Trizol (Invitrogen) and quantitative polymerase chain reaction was performed with TaqMan assays (Applied Biosystems) for human *GAPDH* and *ROBO1* to *ROBO4*.

Endothelial cell migration

Equimolar huRobo1 siRNA (Hs_Robo1_11_HP; Qiagen), huRobo4 siRNA (Hs_Robo4_1_HP), or AllStars Negative Control siRNA transfection complexes were formed according to standard protocol and added to human umbilical vein endothelial cells (Lonza). Companion dishes were prepared to assess knockdown of gene expression. Forty-eight hours later, cells were serum-starved, and 30,000 cells were seeded per fibronectin-coated 6.5-mm Transwell filters with an 8-μm pore size (Costar). Cells were allowed to migrate to 2 nM VEGF in the presence of 10 nM Slit2N or Mock for 20 hours. Filters were removed, migrated cells were counterstained, and eight high-power fields per filter were counted. Relative migration over unstimulated was determined, and data are presented as mean ± SEM of at least three independent experiments performed in at least triplicate.

Statistical analysis

The Student's *t* test, log rank test, or analysis of variance with post hoc tests, where appropriate, was used to assess statistical significance. A P value of <0.05 was considered statistically significant.

Supplementary Material

Refer to Web version on PubMed Central for supplementary material.

REFERENCES AND NOTES

1. Perdue ML, Swayne DE. Public health risk from avian influenza viruses. Avian Dis 2005;49:317–327. [PubMed: 16252482]
2. Bossi P, Garin D, Guihot A, Gay F, Crance JM, Debord T, Autran B, Bricaire F. Bioterrorism: Management of major biological agents. Cell. Mol. Life Sci 2006;63:2196–2212. [PubMed: 16964582]
3. De Jong JC, Rimmelzwaan GF, Fouchier RA, Osterhaus AD. Influenza virus: A master of metamorphosis. J. Infect 2000;40:218–228. [PubMed: 10908015]
4. Morse SS, Garwin RL, Olsiewski PJ. Public health. Next flu pandemic: What to do until the vaccine arrives? Science 2006;314:929. [PubMed: 17095681]
5. Hsieh YC, Wu TZ, Liu DP, Shao PL, Chang LY, Lu CY, Lee CY, Huang FY, Huang LM. Influenza pandemics: Past, present and future. J. Formos. Med. Assoc 2006;105:1–6. [PubMed: 16440064]
6. Hackett CJ. Innate immune activation as a broad-spectrum biodefense strategy: Prospects and research challenges. J. Allergy Clin. Immunol 2003;112:686–694. [PubMed: 14564345]
7. Nathan C. Points of control in inflammation. Nature 2002;420:846–852. [PubMed: 12490957]
8. Aird WC. The role of the endothelium in severe sepsis and multiple organ dysfunction syndrome. Blood 2003;101:3765–3777. [PubMed: 12543869]
9. Morens DM, Fauci AS. Dengue and hemorrhagic fever: A potential threat to public health in the United States. JAMA 2008;299:214–216. [PubMed: 18182605]
10. Ware LB, Matthay MA. The acute respiratory distress syndrome. N. Engl. J. Med 2000;342:1334–1349. [PubMed: 10793167]

11. Abraham E, Laterre PF, Garbino J, Pingleton S, Butler T, Dugernier T, Margolis B, Kudsk K, Zimmerli W, Anderson P, Reynaert M, Lew D, Lesslauer W, Passe S, Cooper P, Burdeska A, Modi M, Leighton A, Salgo M, Van der Auwera P. Lenercept Study Group. Lenercept (p55 tumor necrosis factor receptor fusion protein) in severe sepsis and early septic shock: A randomized, double-blind, placebo-controlled, multicenter phase III trial with 1,342 patients. Crit. Care Med 2001;29:503–510. [PubMed: 11373411]
12. Crum NF, Lederman ER, Wallace MR. Infections associated with tumor necrosis factor-α antagonists. Medicine 2005;84:291–302. [PubMed: 16148729]
13. Cronin L, Cook DJ, Carlet J, Heyland DK, King D, Lansang MA, Fisher CJ Jr. Cortico-steroid treatment for sepsis: A critical appraisal and meta-analysis of the literature. Crit. Care Med 1995;23:1430–1439. [PubMed: 7634816]
14. Atkins MB, Lotze MT, Dutcher JP, Fisher RI, Weiss G, Margolin K, Abrams J, Sznol M, Parkinson D, Hawkins M, Paradise C, Kunkel L, Rosenberg SA. High-dose recombinant interleukin 2 therapy for patients with metastatic melanoma: Analysis of 270 patients treated between 1985 and 1993. J. Clin. Oncol 1999;17:2105–2116. [PubMed: 10561265]
15. Jones CA, London NR, Chen H, Park KW, Sauvaget D, Stockton RA, Wythe JD, Suh W, Larrieu-Lahargue F, Mukouyama YS, Lindblom P, Seth P, Frias A, Nishiya N, Ginsberg MH, Gerhardt H, Zhang K, Li DY. Robo4 stabilizes the vascular network by inhibiting pathologic angiogenesis and endothelial hyperpermeability. Nat. Med 2008;14:448–453. [PubMed: 18345009]
16. Jones CA, Nishiya N, London NR, Zhu W, Sorensen LK, Chan AC, Lim CJ, Chen H, Zhang Q, Schultz PG, Hayallah AM, Thomas KR, Famulok M, Zhang K, Ginsberg MH, Li DY. Slit2–Robo4 signalling promotes vascular stability by blocking Arf6 activity. Nat. Cell Biol 2009;11:1325–1331. [PubMed: 19855388]
17. Huminiecki L, Gorn M, Suchting S, Poulsom R, Bicknell R. Magic roundabout is a new member of the roundabout receptor family that is endothelial specific and expressed at sites of active angiogenesis. Genomics 2002;79:547–552. [PubMed: 11944987]
18. Park KW, Morrison CM, Sorensen LK, Jones CA, Rao Y, Chien CB, Wu JY, Urness LD, Li DY. Robo4 is a vascular-specific receptor that inhibits endothelial migration. Dev. Biol 2003;261:251–267. [PubMed: 12941633]
19. Dinarello CA. Proinflammatory and anti-inflammatory cytokines as mediators in the pathogenesis of septic shock. Chest 1997;112:321S, 329S. [PubMed: 9400897]
20. Chédotal A. Slits and their receptors. Adv. Exp. Med. Biol 2007;621:65–80. [PubMed: 18269211]
21. Dejana E, Orsenigo F, Lampugnani MG. The role of adherens junctions and VE-cadherin in the control of vascular permeability. J. Cell Sci 2008;121:2115–2122. [PubMed: 18565824]
22. Vestweber D. VE-cadherin: The major endothelial adhesion molecule controlling cellular junctions and blood vessel formation. Arterioscler. Thromb. Vasc. Biol 2008;28:223–232. [PubMed: 18162609]
23. Potter MD, Barbero S, Cheresh DA. Tyrosine phosphorylation of VE-cadherin prevents binding of p120- and β-catenin and maintains the cellular mesenchymal state. J. Biol. Chem 2005;280:31906–31912. [PubMed: 16027153]
24. Xiao K, Garner J, Buckley KM, Vincent PA, Chiasson CM, Dejana E, Faundez V, Kowalczyk AP. p120-catenin regulates clathrin-dependent endocytosis of VE-cadherin. Mol. Biol. Cell 2005;16:5141–5151. [PubMed: 16120645]
25. Gampel A, Moss L, Jones MC, Brunton V, Norman JC, Mellor H. VEGF regulates the mobilization of VEGFR2/KDR from an intracellular endothelial storage compartment. Blood 2006;108:2624–2631. [PubMed: 16638931]
26. Matute-Bello G, Frevert CW, Martin TR. Animal models of acute lung injury. Am. J. Physiol. Lung Cell. Mol. Physiol 2008;295:L379–L399. [PubMed: 18621912]
27. Corada M, Liao F, Lindgren M, Lampugnani MG, Breviario F, Frank R, Muller WA, Hicklin DJ, Bohlen P, Dejana E. Monoclonal antibodies directed to different regions of vascular endothelial cadherin extracellular domain affect adhesion and clustering of the protein and modulate endothelial permeability. Blood 2001;97:1679–1684. [PubMed: 11238107]
28. Hubbard WJ, Choudhry M, Schwacha MG, Kerby JD, Rue LW III, Bland KI, Chaudry IH. Cecal ligation and puncture. Shock 2005;24:52–57. [PubMed: 16374373]

29. de Jong MD, Simmons CP, Thanh TT, Hien VM, Smith GJ, Chau TN, Hoang DM, Chau NV, Khanh TH, Dong VC, Qui PT, Cam BV, Ha do Q, Guan Y, Peiris JS, Chinh NT, Hien TT, Farrar J. Fatal outcome of human influenza A (H5N1) is associated with high viral load and hypercytokinemia. Nat. Med 2006;12:1203–1207. [PubMed: 16964257]
30. Kobasa D, Jones SM, Shinya K, Kash JC, Copps J, Ebihara H, Ebihara H, Hatta Y, Kim JH, Halfmann P, Hatta M, Feldmann F, Alimonti JB, Fernando L, Li Y, Katze MG, Feldmann H, Kawaoka Y. Aberrant innate immune response in lethal infection of macaques with the 1918 influenza virus. Nature 2007;445:319–323. [PubMed: 17230189]
31. Abdel-Ghafar, AN.; Chotpitayasunondh, T.; Gao, Z.; Hayden, FG.; Nguyen, DH.; de Jong, MD.; Naghdaliyev, A.; Peiris, JS.; Shindo, N.; Soeroso, S.; Uyeki, TM. Writing Committee of the Second World Health Organization Consultation on Clinical Aspects of Human Infection with Avian Influenza A (H5N1) Virus. Update on avian influenza A (H5N1) virus infection in humans; N. Engl. J. Med. 2008. p. 261-273.
32. Sepkowitz KA. Forever unprepared—The predictable unpredictability of pathogens. N. Engl. J. Med 2009;361:120–121. [PubMed: 19587337]
33. Layne SP, Monto AS, Taubenberger JK. Pandemic influenza: An inconvenient mutation. Science 2009;323:1560–1561. [PubMed: 19299601]
34. Seeger M, Tear G, Ferres-Marco D, Goodman CS. Mutations affecting growth cone guidance in Drosophila: Genes necessary for guidance toward or away from the midline. Neuron 1993;10:409–426. [PubMed: 8461134]
35. Xian J, Clark KJ, Fordham R, Pannell R, Rabbitts TH, Rabbitts PH. Inadequate lung development and bronchial hyperplasia in mice with a targeted deletion in the *Dutt1/Robo1* gene. Proc. Natl. Acad. Sci. U.S.A 2001;98:15062–15066. [PubMed: 11734623]
36. Grieshammer U, Le M, Plump AS, Wang F, Tessier-Lavigne M, Martin GR. SLIT2-mediated ROBO2 signaling restricts kidney induction to a single site. Dev. Cell 2004;6:709–717. [PubMed: 15130495]
37. Sabatier C, Plump AS, Le M, Brose K, Tamada A, Murakami F, Leem EY, Tessier-Lavigne M. The divergent Robo family protein Rig-1/Robo3 is a negative regulator of Slit responsiveness required for midline crossing by commissural axons. Cell 2004;117:157–169. [PubMed: 15084255]
38. Qureshi ST, Medzhitov R. Toll-like receptors and their role in experimental models of microbial infection. Genes Immun 2003;4:87–94. [PubMed: 12618855]
39. Wu JY, Feng L, Park HT, Havlioglu N, Wen L, Tang H, Bacon KB, Jiang Z, Zhang X, Rao Y. The neuronal repellent Slit inhibits leukocyte chemotaxis induced by chemotactic factors. Nature 2001;410:948–952. [PubMed: 11309622]
40. Mei SH, McCarter SD, Deng Y, Parker CH, Liles WC, Stewart DJ. Prevention of LPS-induced acute lung injury in mice by mesenchymal stem cells overexpressing angiopoietin 1. PLoS Med 2007;4:e269. [PubMed: 17803352]
41. Seth P, Lin Y, Hanai J, Shivalingappa V, Duyao MP, Sukhatme VP. Magic roundabout, a tumor endothelial marker: Expression and signaling. Biochem. Biophys. Res. Commun 2005;332:533–541. [PubMed: 15894287]
42. Sheldon H, Andre M, Legg JA, Heal P, Herbert JM, Sainson R, Sharma AS, Kitajewski JK, Heath VL, Bicknell R. Active involvement of Robo1 and Robo4 in filopodia formation and endothelial cell motility mediated via WASP and other actin nucleation-promoting factors. FASEB J 2009;23:513–522. [PubMed: 18948384]
43. Hu H. Cell-surface heparan sulfate is involved in the repulsive guidance activities of Slit2 protein. Nat. Neurosci 2001;4:695–701. [PubMed: 11426225]
44. Hohenester E, Hussain S, Howitt JA. Interaction of the guidance molecule Slit with cellular receptors. Biochem. Soc. Trans 2006;34:418–421. [PubMed: 16709176]
45. Steigemann P, Molitor A, Fellert S, Jäckle H, Vorbrüggen G. Heparan sulfate proteoglycan syndecan promotes axonal and myotube guidance by Slit/Robo signaling. Curr. Biol 2004;14:225–230. [PubMed: 14761655]
46. Suchting S, Heal P, Tahtis K, Stewart LM, Bicknell R. Soluble Robo4 receptor inhibits in vivo angiogenesis and endothelial cell migration. FASEB J 2005;19:121–123. [PubMed: 15486058]
47. Vestweber D, Winderlich M, Cagna G, Nottebaum AF. Cell adhesion dynamics at endothelial junctions: VE-cadherin as a major player. Trends Cell Biol 2009;19:8–15. [PubMed: 19010680]

48. Wallez Y, Huber P. Endothelial adherens and tight junctions in vascular homeostasis, inflammation and angiogenesis. Biochim. Biophys. Acta 2008;1778:794–809. [PubMed: 17961505]

49. Gavard J, Gutkind JS. VEGF controls endothelial-cell permeability by promoting the β-arrestin-dependent endocytosis of VE-cadherin. Nat. Cell Biol 2006;8:1223–1234. [PubMed: 17060906]

50. Ferreira AM, McNeil CJ, Stallaert KM, Rogers KA, Sandig M. Interleukin-1β reduces transcellular monocyte diapedesis and compromises endothelial adherens junction integrity. Microcirculation 2005;12:563–579. [PubMed: 16207629]

51. Angelini DJ, Hyun SW, Grigoryev DN, Garg P, Gong P, Singh IS, Passaniti A, Hasday JD, Goldblum SE. TNF-α increases tyrosine phosphorylation of vascular endothelial cadherin and opens the paracellular pathway through fyn activation in human lung endothelia. Am. J. Physiol. Lung Cell. Mol. Physiol 2006;291:L1232–L1245. [PubMed: 16891393]

52. Gavard J, Patel V, Gutkind JS. Angiopoietin-1 prevents VEGF-induced endothelial permeability by sequestering Src through mDia. Dev. Cell 2008;14:25–36. [PubMed: 18194650]

53. Villa P, Sartor G, Angelini M, Sironi M, Conni M, Gnocchi P, Isetta AM, Grau G, Buurman W, van Tits LJ. Pattern of cytokines and pharmacomodulation in sepsis induced by cecal ligation and puncture compared with that induced by endotoxin. Clin. Diagn. Lab. Immunol 1995;2:549–553. [PubMed: 8548533]

54. Coltel N, Combes V, Hunt NH, Grau GE. Cerebral malaria—A neurovascular pathology with many riddles still to be solved. Curr. Neurovasc. Res 2004;1:91–110. [PubMed: 16185187]

55. London NR, Whitehead KJ, Li DY. Endogenous endothelial cell signaling systems maintain vascular stability. Angiogenesis 2009;12:149–158. [PubMed: 19172407]

56. Gomes RN, Figueiredo RT, Bozza FA, Pacheco P, Amâncio RT, Laranjeira AP, Castro-Faria-Neto HC, Bozza PT, Bozza MT. Increased susceptibility to septic and endotoxic shock in monocyte chemoattractant protein 1/cc chemokine ligand 2-deficient mice correlates with reduced interleukin 10 and enhanced macrophage migration inhibitory factor production. Shock 2006;26:457–463. [PubMed: 17047515]

57. Moitra J, Sammani S, Garcia JG. Re-evaluation of Evans Blue dye as a marker of albumin clearance in murine models of acute lung injury. Transl. Res 2007;150:253–265. [PubMed: 17900513]

58. Gupta N, Su X, Popov B, Lee JW, Serikov V, Matthay MA. Intrapulmonary delivery of bone marrow-derived mesenchymal stem cells improves survival and attenuates endotoxin-induced acute lung injury in mice. J. Immunol 2007;179:1855–1863. [PubMed: 17641052]

59. Sidwell RW, Bailey KW, Wong MH, Barnard DL, Smee DF. In vitro and in vivo influenza virus-inhibitory effects of viramidine. Antiviral Res 2005;68:10–17. [PubMed: 16087250]

60. Metzger RJ, Klein OD, Martin GR, Krasnow MA. The branching programme of mouse lung development. Nature 2008;453:745–750. [PubMed: 18463632]

61. Collins SJ, Ruscetti FW, Gallagher RE, Gallo RC. Terminal differentiation of human promyelocytic leukemia cells induced by dimethyl sulfoxide and other polar compounds. Proc. Natl. Acad. Sci. U.S.A 1978;75:2458–2462. [PubMed: 276884]

62. Zimmerman GA, McIntyre TM, Prescott SM. Thrombin stimulates the adherence of neutrophils to human endothelial cells in vitro. J. Clin. Invest 1985;76:2235–2246. [PubMed: 4077977]

63. Acknowledgments: We thank D. Lim for graphical assistance and K. Thomas, M. Sanguinetti, A. Welm, C. Murtaugh, S. Odelberg, and S. Stanley for critical reading of this manuscript. Funding: National Heart, Lung, and Blood Institute (NHLBI); National Institute of Allergy and Infectious Diseases (NIAID); Rocky Mountain Regional Center of Excellence in Biodefense and Emerging Infectious Disease; Juvenile Diabetes Research Foundation; HA and Edna Benning Foundation; American Asthma Foundation; National Center for Research Resources Public Health Services research grant UL1-RR025764; and Department of Defense. D.Y.L. is a Burroughs Wellcome Foundation Clinical Scientist in Translational Research and an Established Investigator of the American Heart Association. N.R.L., M.C.P.S., and A.C.C. were supported, respectively, by the Ruth L. Kirschstein National Research Service Award, T-32 Hematology Training Grant, and training grant T32-GM007464. This work was also supported by NIAID contract NO1-AI-15435 (C.W.D. and D.L.B.); a NIH Merit Award 5R37 HL44525-20 (G.A.Z.); and the Sarnoff Cardiovascular Research Foundation Scholar Award, NIH-NHLBI (K08), and the Pulmonary Hypertension Association (D.M.G.). F.A.B. is a research scholar supported by Conselho Nacional de Desenvolvimento Científico e Tecnológico (CNPq, Brazil).

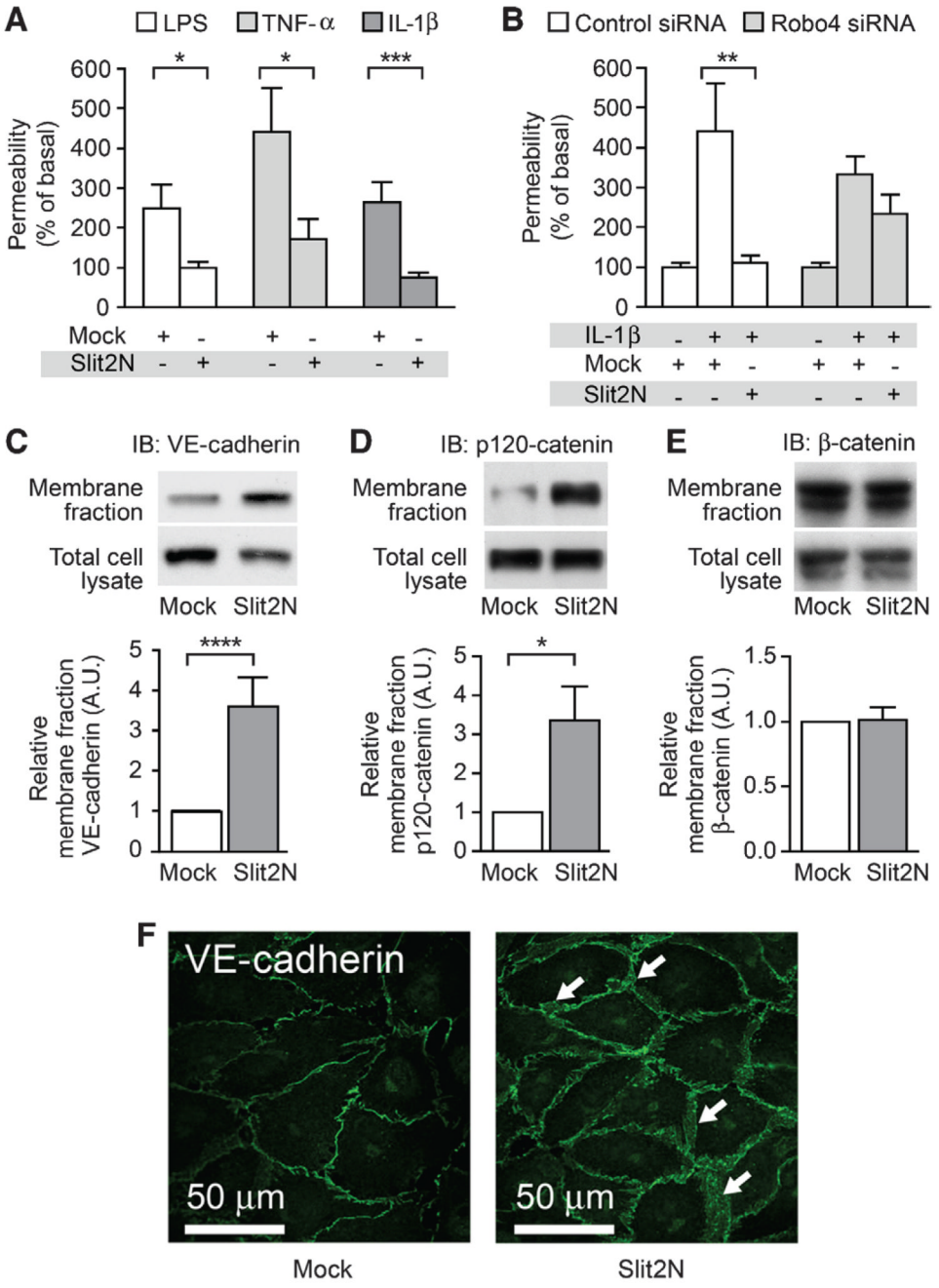

Fig. 1.

Slit2N stabilizes the endothelium in vitro by enhancing VE-cadherin localization at the cell surface. (**A**) In vitro permeability was measured in HMVEC-lung cells stimulated with LPS, TNF-α, or IL-1β in the presence of Mock (see Materials and Methods) or Slit2N. (**B**) Robo4 or control siRNA knockdown-treated HMVEC-lung cells were stimulated with IL-1β in the presence of Mock or Slit2N to assess permeability in vitro. (**C** to **E**) HMVEC-lung cells were treated with Mock or Slit2N and subjected to membrane fractionation and subsequent immunoblotting for VE-cadherin (C), p120-catenin (D), or β-catenin (E). (**F**) HMVEC-lung cells were stimulated with Mock or Slit2N and subjected to immunofluorescence for VE-cadherin (green). White arrows, areas of enhanced VE-cadherin cell surface localization. For

all experiments, $n \geq 3$, and error bars represent SEM. *$P < 0.05$, **$P < 0.01$, ***$P < 0.005$, ****$P < 0.001$.

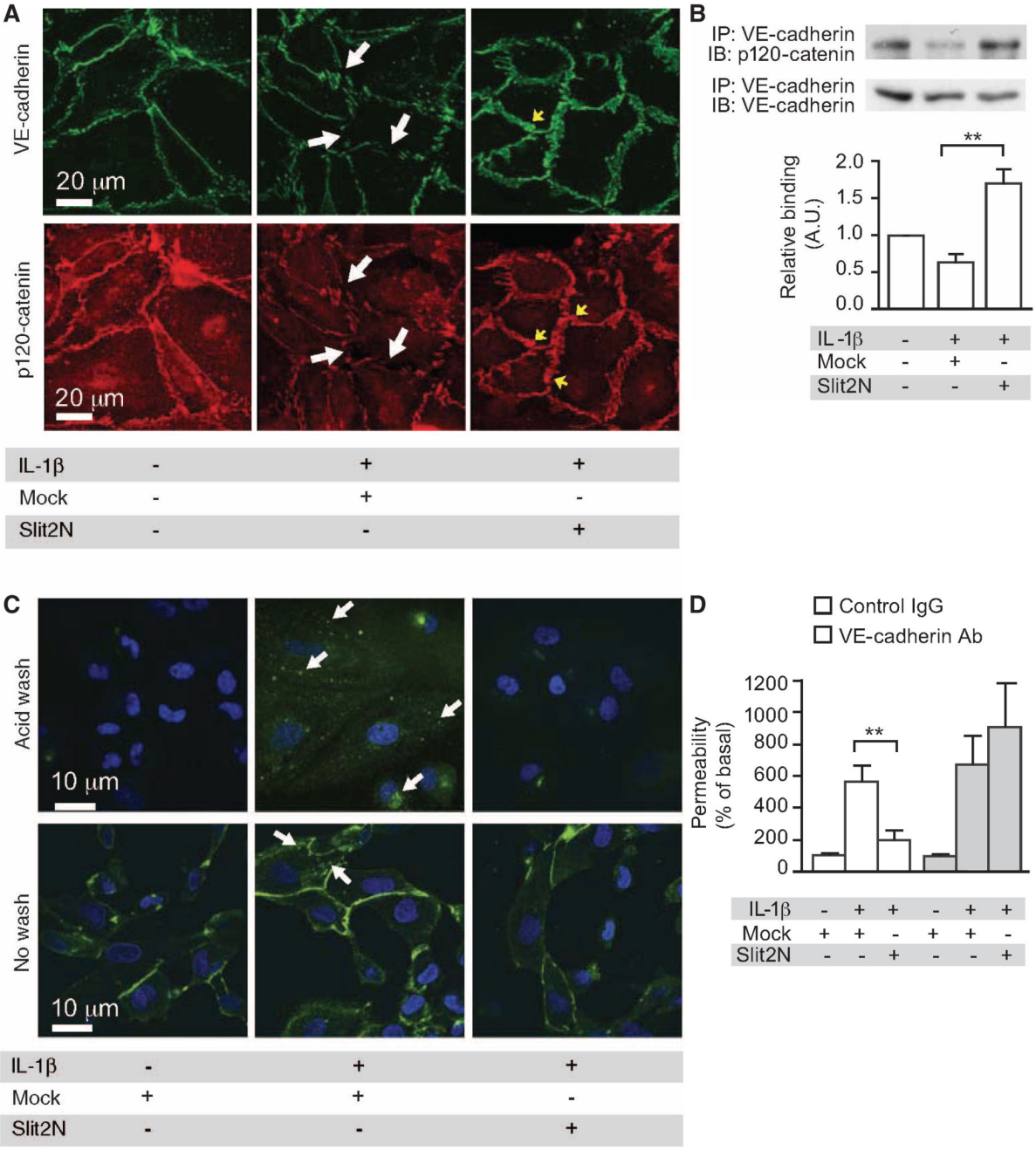

Fig. 2.

Slit2N enhances a VE-cadherin–p120-catenin interaction in vitro. (**A**) HMVEC-lung cells were stimulated with IL-1β in the presence of Mock or Slit2N and immunostained for VE-cadherin and p120-catenin. White arrows, cell surface areas lacking VE-cadherin or p120-catenin in Mock-treated cells; yellow arrows, areas of enhanced cell surface localization of VE-cadherin or p120-catenin in Slit2N-treated cells. (**B**) HMVEC-lung cells were stimulated with IL-1β in the presence of Mock or Slit2N. Lysates were subjected to immunoprecipitation for VE-cadherin followed by immunoblot for p120-catenin and VE-cadherin. (**C**) HMVEC-lung cells were labeled with an antibody to VE-cadherin and stimulated with IL-1β in the presence of Mock or Slit2N. Cells were acid-washed to strip the surface-bound VE-cadherin (top row).

VE-cadherin internalization (green) was assessed. White arrows, areas of internalization. (**D**) In vitro permeability was measured in the presence of a control IgG or VE-cadherin antibody (Ab). For all experiments, $n \geq 3$, and error bars represent SEM. $^{**}P < 0.01$.

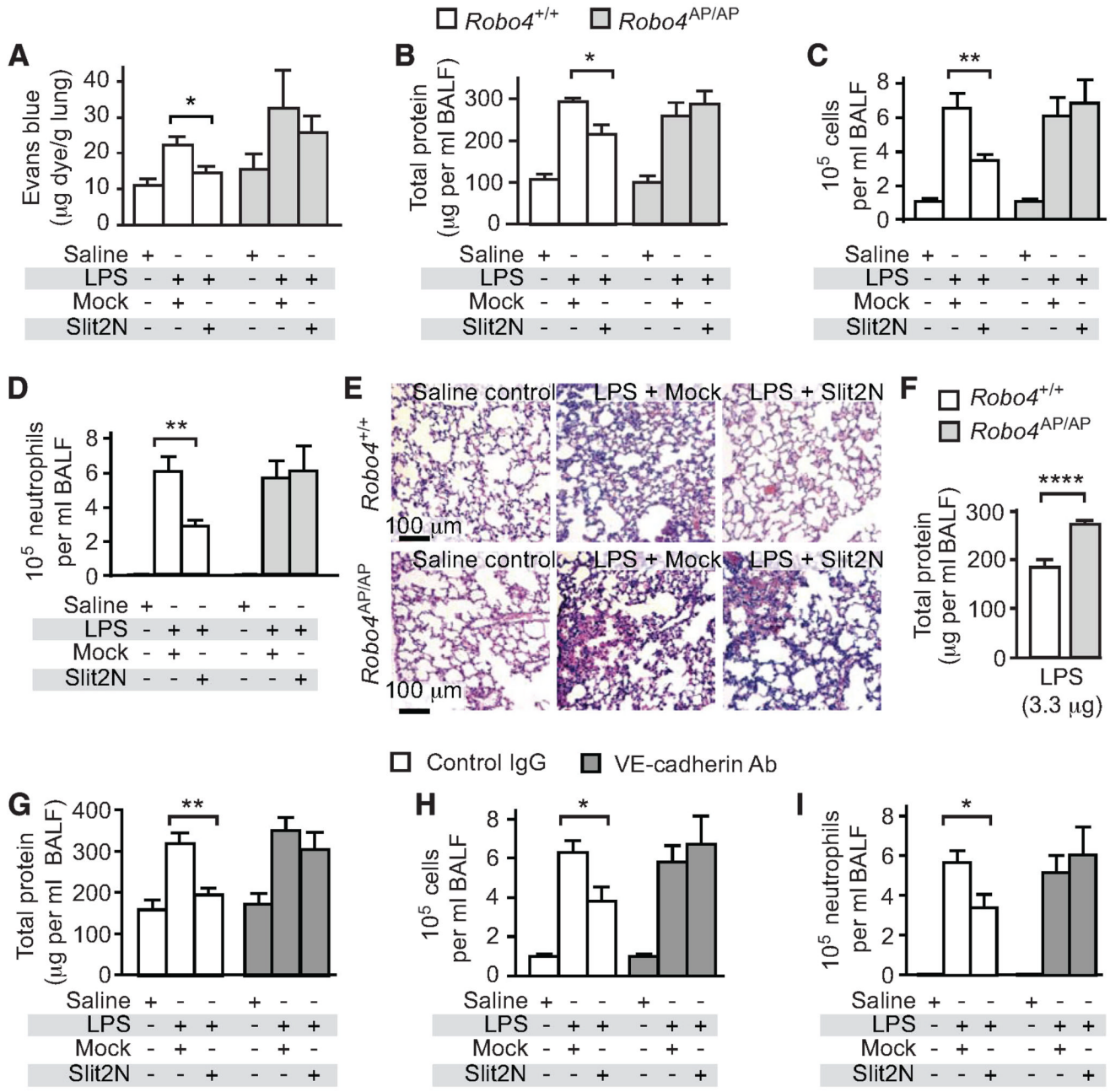

Fig. 3.

Slit2N inhibits LPS-induced permeability, protein exudates, and cell infiltrates in vivo. (**A**) *Robo4*$^{+/+}$ and *Robo4*$^{AP/AP}$ mice were given an intravenous injection of Mock or Slit2N followed by intratracheal instillation of LPS (10 μg). Mice later received an intravenous injection of EBA, and EBA accumulation in the lungs was used to assess vascular permeability ($n \geq 4$). (**B** to **D**) Twenty-four hours after LPS administration, bronchoalveolar lavages were obtained and assessed for protein content (B), total inflammatory cell accumulation (C), or neutrophil accumulation (saline value is too low to be visible) (D) ($n \geq 5$). (**E**) H&E staining was performed on lung sections from mice exposed to LPS in the presence of Mock or Slit2N. (**F**) Protein exudates measured in mice treated with 3.3 μg of LPS ($n = 5$). (**G** to **I**) Mice were

given an intravenous injection of Mock or Slit2N with control or VE-cadherin–blocking antibody followed by intratracheal instillation of LPS. Bronchoalveolar lavages were obtained and assessed for protein content (G), total inflammatory cell accumulation (H), or neutrophil accumulation (I) ($n \geq 5$). Error bars represent SEM. *$P < 0.05$, **$P < 0.01$, ****$P < 0.001$.

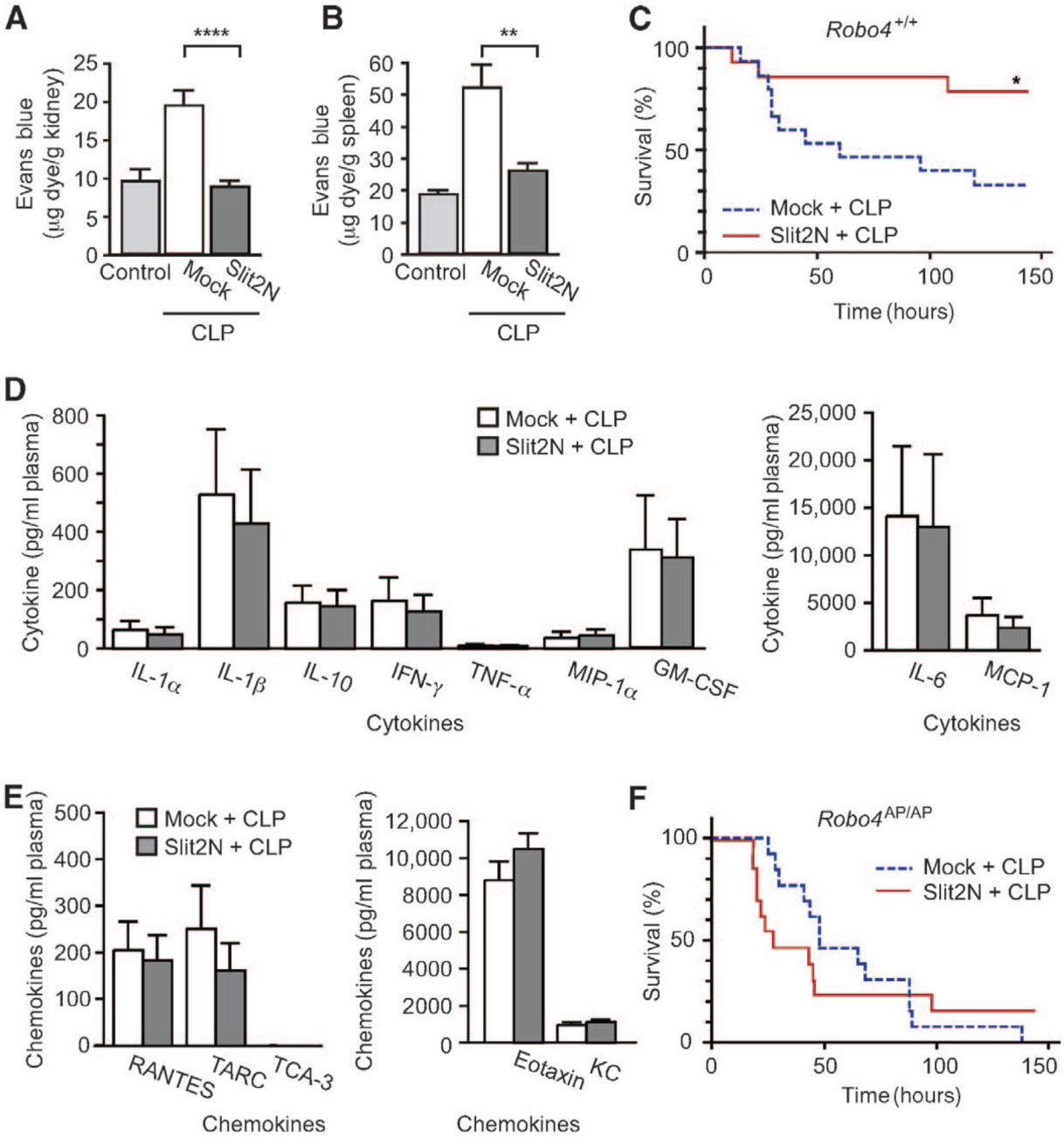

Fig. 4.

Slit2N reduces permeability and mortality in a CLP model of sepsis. (**A** and **B**) Mice were subjected to CLP or sham operation and then given an intravenous injection of EBA. EBA accumulation was measured in the kidney (A) or spleen (B) to assess vascular permeability ($n = 5$). (C) *Robo4*$^{+/+}$ mice were subjected to CLP and treated with Mock or Slit2N, and survival was assessed (Mock-treated, $n = 15$; Slit2N-treated, $n = 14$). (**D** and **E**) Cytokine (D) and chemokine (E) concentrations in the serum of Mock- or Slit2N-treated CLP mice ($n = 6$). (**F**) *Robo4*$^{AP/AP}$ mice were subjected to CLP and treated with Mock or Slit2N, and survival was assessed (Mock-treated, $n = 13$; Slit2N-treated, $n = 13$). Error bars represent SEM. *$P < 0.05$, **$P < 0.01$, ****$P < 0.001$.

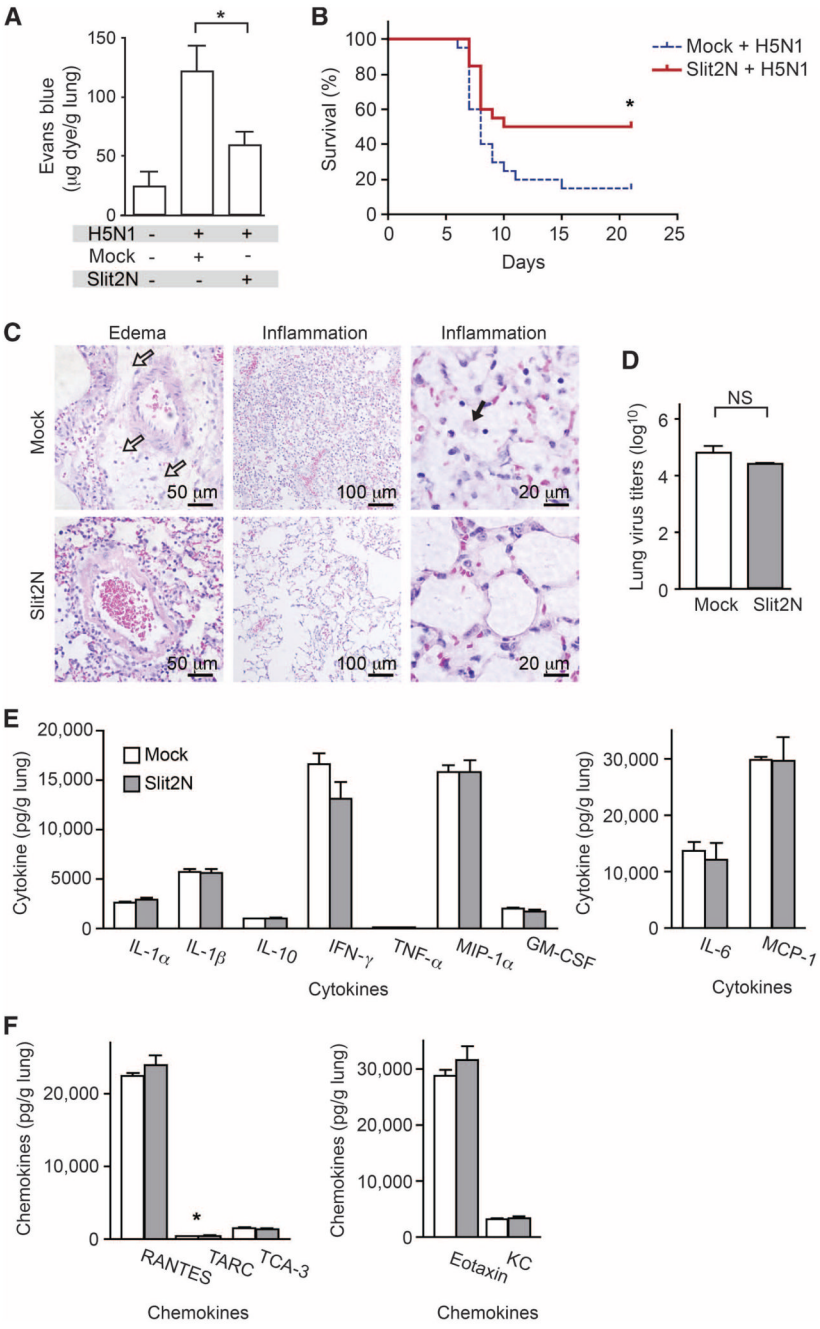

Fig. 5.

Slit2N reduces mortality in models of H5N1 infection. (**A**) BALB/c mice were infected intranasally with H5N1 virus. Mice were given an intravenous injection of EBA, and EBA accumulation was measured in the lungs to assess vascular permeability ($n = 5$). (**B**) Mouse survival after H5N1 infection (Mock-treated, $n = 20$; Slit2N-treated, $n = 20$). (**C**) H&E staining was performed on lung sections from H5N1-infected mice 6 days after infection. White arrows in the top left panel show accumulation of edema fluid around a pulmonary arteriole. The top middle panel demonstrates exuberant alveolar inflammation. The black arrow in the top right panel shows the presence of foamy macrophages. (**D**) H5N1 viral titers were measured 6 days after infection ($n = 3$ groups of pooled mice). (**E** and **F**) Cytokine (E) or chemokine (F)

concentrations measured in lung homogenates 6 days after infection ($n = 3$ groups of pooled mice). *$P < 0.05$. NS, not significant.

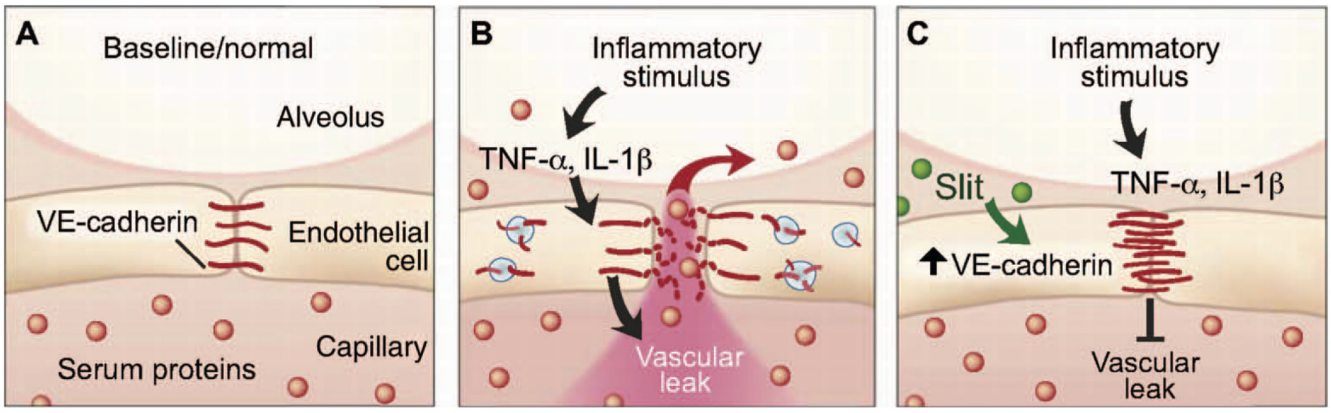

Fig. 6.

Slit reduces vascular leak caused by multiple inflammatory stimuli through enhancing VE-cadherin at the cell surface. (**A**) Under normal conditions, alveolar capillaries are semipermeable. (**B**) Inflammatory stimuli cause a large release of cytokines, leading to internalization of VE-cadherin and disruption of barrier function. This results in vascular leak and accumulation of protein-rich edema fluid in the alveolar space. (**C**) Slit enhances vascular barrier function against multiple cytokines by enhancing VE-cadherin at the cell surface.